APPLIED PHYSICS LETTERS **107**, 163107 (2015)

Discrimination of molecular thin films by surface-sensitive time-resolved optical spectroscopy

Simone Peli,[1,2] Nicola Nembrini,[1,2,3] Francesco Damin,[4] Marcella Chiari,[4] Claudio Giannetti,[1,2] Francesco Banfi,[1,2] and Gabriele Ferrini[1,2,a)]

[1]*Dipartimento di Matematica e Fisica, Università Cattolica del Sacro Cuore, Brescia I-25121, Italy*
[2]*Interdisciplinary Laboratories for Advanced Materials Physics (iLamp), Università Cattolica del Sacro Cuore, Brescia I-25121, Italy*
[3]*Dipartimento di Fisica, Università degli Studi di Milano, Milano I-20122, Italy*
[4]*Istituto di Chimica del Riconoscimento Molecolare, CNR, Milano, Italy*

(Received 24 May 2015; accepted 30 September 2015; published online 21 October 2015)

An optical discrimination technique, tailored to nanometric-sized, low optical absorbance molecular complexes adhering to thin metal films, is proposed and demonstrated. It is based on a time-resolved evanescent-wave detection scheme in conjunction with hierarchical cluster analysis and principal value decomposition. The present approach aims to differentiate among molecular films based on statistical methods, without using previous detailed knowledge of the physical mechanisms responsible for the detected signal. The technique is open to integration in lab-on-a-chip architectures and nanoscopy platforms for applications ranging from medical screening to material diagnostics. © *2015 Author(s). All article content, except where otherwise noted, is licensed under a Creative Commons Attribution 3.0 Unported License*. [http://dx.doi.org/10.1063/1.4934216]

Optical detection of biomolecules plays a pivotal role in modern biophysics[1,2] and biophotonics,[3–5] especially for molecular complexes immobilized on surfaces.[6] Optical spectroscopy and fluorescence emission are routinely used to investigate structural conformation changes of molecular beacons on decorated surfaces[7,8] and detect surface-bound engineered polypeptides.[9] Since the molecular fingerprint is encoded in either the spectral reflectance/transmittance or the spectral fluorescence emission, optical spectroscopies based on multi-wavelength detection have been widely employed. Despite their success, conventional optical spectroscopies suffer some major drawbacks, such as the lack of specific surface sensitivity and time-resolved capabilities, i.e., the potential to follow transient molecular excitations initiated by an external trigger. In order to overcome some of the above-mentioned shortcomings, we developed a molecular discrimination technique, based on time-resolved evanescent wave[10] optical spectroscopy and data mining techniques.

The experiment is based on a pump and probe optical scheme to investigate biomolecular layers with typical vertical dimensions of the order of less than 10 nm, 2 orders of magnitude smaller than the optical wavelength. The molecular layer is bound to an Au thin film deposited on the hypotenuse of a glass prism. A pump laser pulse excites the Au film. A time-delayed evanescent wave probe pulse, created at the glass-air interface of a prism in the Kretschmann configuration,[11] probes a volume comprising the Au film and the molecular layers (see the inset of Fig. 1). The relative reflectivity variation of the probe pulse is recorded as a function of the time delay from the pump pulse arrival.

While time-resolved spectroscopy techniques are not new to biochemistry,[12] they are usually employed to study the relaxation behavior of *known* molecular species. Here, we use the information contained in time-resolved reflectivity variation to sort out the differences among different molecular aggregates on thin metallic films. To highlight the specificity of the present approach, it is appropriate to make comparisons with already developed optical surface sensitive techniques: second harmonic generation spectroscopy (SHGS),[13] sum-frequency generation vibrational spectroscopy (SFG-VS),[14] surface cavity ring-down spectroscopy (s-CRDS),[15,16] and attenuated total reflection (ATR) infrared spectroscopy.[17] These are well established surface-sensitive optical techniques, each with dedicated theoretical methods already developed and widely used in biophysics. Each of

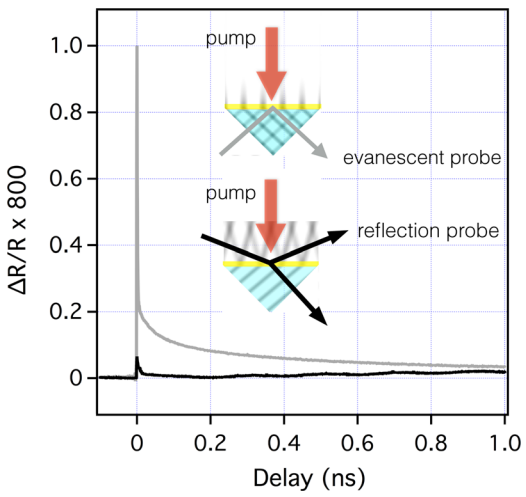

FIG. 1. Relative reflectivity variation of the optical probe pulses vs time delay from the optical pump pulse in the reflection (black line) and evanescent (gray line) configurations. Insets: probe configurations for a gold coated fused silica prism in the evanescent wave scheme (top panel) and reflection scheme (bottom panel). The probe wavefronts (light gray) are shown in the prism (light blue) and in the vacuum. Note the evanescent probe with the external wavefronts orthogonal to the prism surface (top panel).

a)Electronic mail: gabriele.ferrini@unicatt.it

these techniques allows one to investigate the orientation of surface molecules and gather important insights into their chemistry.

SHGS and SFG-VS are nonlinear techniques requiring relatively high intensity laser pulses. The signal may originate from bulk multipolar contributions near the surface of a centrosymmetric or isotropic medium. In addition, contributions may arise from thin metal films supporting the investigated molecular layers. For these reasons, caution must be taken, and the use of theoretical models is mandatory in interpreting data.[14] ATR and s-CRDS are based on evanescent waves and linear absorption. The latest refinements in CRDS with stabilized frequency combs reached exquisite sensitivity,[16] but both are spectroscopic techniques that do not encompass time resolved capabilities. The approach proposed in this work combines the time resolved capability and surface sensitivity of non-linear techniques with linear probe absorption as in s-CRDS or ATR *at a single wavelength*. Instead of relying on spectral absorption features, we use the complex interplay of physical mechanisms that lead to the variation of absorption after pump excitation as a distinctive feature of the molecular layers under investigation.[18] Moreover, as in s-CRDS, the polarization information could be used to determine the molecular orientation.[15]

The time-resolved spectra are analyzed using two approaches: (1) a hierarchical binary cluster tree dendrogram built using a Euclidean distance (Ward method)[19] and (2) a singular value decomposition (SVD) analysis.[20] These approaches are compared against the standard analysis of the time-dynamics of molecular complexes based on the sum of exponentially decaying functions and are shown to provide the best performance.

The pump and probe laser pulses are generated by two synchronized femtosecond fiber lasers with a repetition rate of 100 MHz and a pulse time width of 120 fs. The fundamental wavelength of 1560 nm of the first laser is used as a pump, while the second harmonic at 780 nm of the second laser is used as a probe. The delay between the pump and probe pulses is obtained by the Asynchronous Optical Sampling (ASOPS) technique.[21] This technique allows one to measure relative reflectivity variation as small as 10^{-6} over a delay window extending from 100 fs to 10 ns.

The experiments are performed on a BK7 prism hypotenuse, where a nominal thickness of 4 nm of gold is evaporated. The gold-coated prism is functionalized with a multifunctional copolymer of dimethylacrylamide (DMA), *N*-acryloyloxysuccinimide (NAS), and 3-(trimethoxysilyl) propyl methacrylate (MAPS)–copoly(DMA-NAS-MAPS)–providing reactive groups suitable for immobilizing molecular structures.[9] The gold coated prism constitutes the reference system. The gold film coated with the copoly (DMA-NAS-MAPS) constitutes our first model. A biotinylated IgG antibody covalently immobilized by the copolymer on the surface of the prism constitutes the second model of our study.[18]

In Fig. 1, we show the signal measured on the reference sample in the evanescent probe configuration, which is 20 times bigger than the signal obtained in the conventional reflection geometry. This result demonstrates the surface-sensitivity of the ASOPS-based time-resolved technique in the evanescent-wave configuration. We point out that both the pump ($\lambda_{pump} = 1560$ nm) and probe ($\lambda_{probe} = 780$ nm) wavelengths are far from the Au surface plasmon resonances, which play no role in the present experiment. This enlarges the range of exploitable coating materials and probe wavelengths, a fact of relevance in view of applications where disparate bio-systems may call for a specific coating material due to technical or cost-related issues. It is important to note that the estimated temperature increase due to pump absorption in our experimental conditions is less than 10 K, and no damage to the biomolecular film is expected.[18]

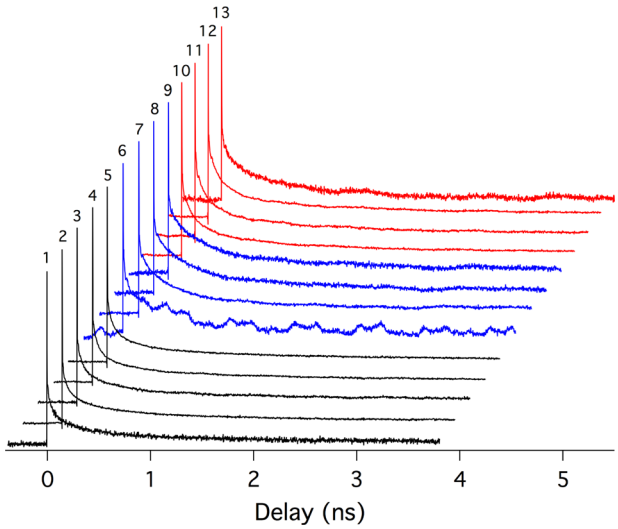

FIG. 2. Relative reflectivity variation of the optical probe pulses vs time delay from the optical pump pulse recorded in the evanescent configuration for Au (black lines), copoly(DMA-NAS-MAPS) (blue lines), and IgG antibody (red lines). The traces have been shifted for clarity.

The variation of the evanescent probe reflection induced by the optical pump has the ubiquitous decaying exponential shape (Fig. 2). The dynamics measured on the different samples looks very similar, the signature of the specific time-response of individual molecular aggregates residing in tiny differences. We use signal analysis methods to extract these differences and exploit them to discriminate among different molecular aggregates.

To illustrate the method, we consider the time resolved measurements relative to three samples: the bare gold film (black lines, from 1 to 5 in Fig. 2); the gold film coated with the copoly(DMA-NAS-MAPS) (blue lines, from 6 to 9 in Fig. 2); the gold film coated with the copoly(DMA-NAS-MAPS) that immobilize the IgG antibody (red lines, from 10 to 13 in Fig. 2).

Since the measurements on the same sample may vary when repeated after some days due to different ambient conditions (temperature and humidity), or because the experiment is carried out at a different spot on the sample, we made multiple sets of measurements for each of the three samples. The total 13 measurements have been organized in a 2000×13 data matrix X. Each column represents a complete experimental trace. Rows map time delays. Note that the traces are affected by evident variations of the noise superposed on the exponential decay dynamic. We included in the analysis even traces that are visually not appealing,

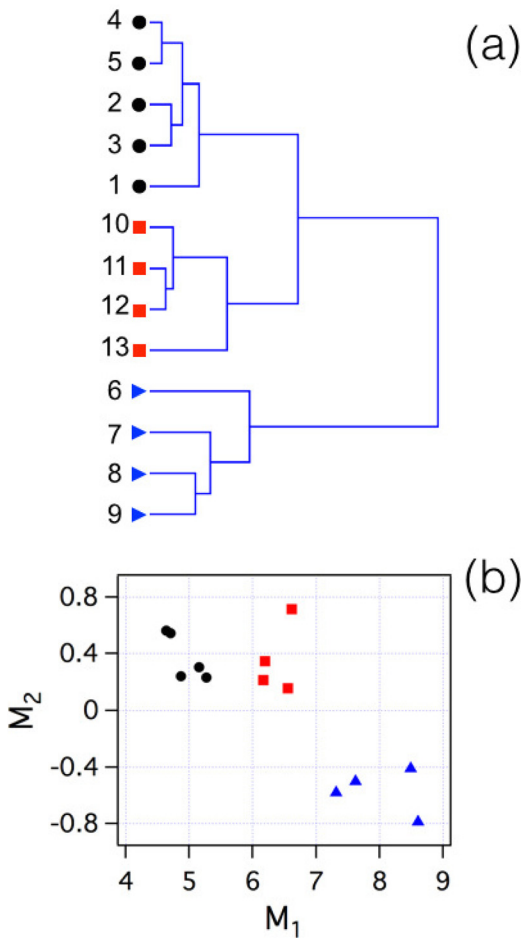

FIG. 3. Data analysis of the traces shown in Fig. 2. (a) Hierarchical Cluster Analysis. Dendrogram obtained using the Ward's method. The horizontal lengths between nodes are proportional to the linkage distance. (b) Single Value Decomposition Analysis. Each point represents the coordinates (M_1,M_2) of a specific trace in the space spanned by the two eigenvectors with the highest eigenvalues. The color code is the same as in Fig. 2. Traces from similar samples are grouped together into separate sets.

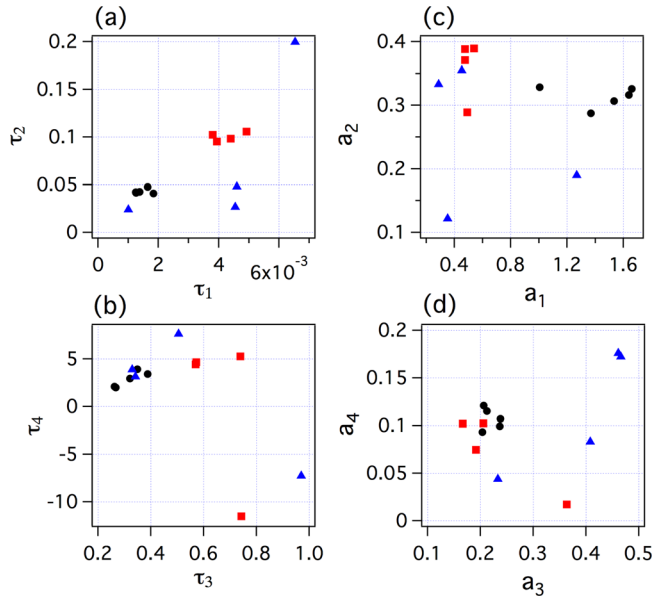

FIG. 4. Grouping based on the parameters used to fit the experimental traces with a four exponential model, needing eight fitting parameters, four decay constants (τ_1, τ_2, τ_3, and τ_4) measured in ns and four normalized amplitudes (a_1, a_2, a_3, and a_4). (a) Each point represents the coordinates (τ_1 and τ_2) of the two shortest decay constants used to fit a specific trace. (b) Each point represents the coordinates (τ_3 and τ_4) of the two longest decay constants. (c) and (d) Each point represents the coordinates of the amplitudes associated with the corresponding decay constants. The presence of negative decay constants for very long decay times (τ_4) do not have physical meaning, being connected to a small increasing trend of the background.[18]

such as trace 6 in Fig. 2, and traces where noise is visually greater than optimum as in traces 1, 8, 9, and 13. The aim is to demonstrate the robustness of the analysis against the presence of external perturbations.

To measure the similarity among spectra, we first adopt cluster analysis to perform an exploratory inspection. Specifically, we aggregate the data using a hierarchical cluster analysis known as Ward's minimum variance method.[19] This is an agglomerative method that clusters data with the criterion to minimize the total within-cluster variance once an appropriate metric has been defined to "measure" the distance among experimental traces. The aim is to reveal the internal similarities among traces and to structure these similarities hierarchically. To calculate the variance, a squared Euclidean distance between traces is used. The results of hierarchical clustering are presented in the dendrogram shown in Fig. 3(a). The data group in three distinct clusters, each associated with one of the three investigated samples, according to the principle that similar samples cluster together because they have similar traces.[18]

SVD[20] is a complementary data analysis approach. SVD is used here to reduce the dimensionality of the data, projecting the data on a reduced eigenvector basis of particular relevance. In this case, clustering emerges when different objects have similar projections.

Entering in more details, the data matrix is expanded in the form $X = USV^T$, where U is a matrix with the same dimensions as X whose columns are the orthonormal basis vectors for the time-resolved measurements and the rows of V contain the coordinates of each measurement projected on the eigenvectors space. S is a diagonal matrix that gives the eigenvalues spectrum, scaling the basis vectors according to their importance in reconstructing the data. The matrix $M = SV^T$ gives the coordinates of the data, so that $X = UM$.

As usual in this context, we reduce the data dimensions by projecting the original data into the subspace spanned by the two eigenvectors with the highest eigenvalues. Visualizing the coordinates as points in a scatter plot (Fig. 3(b)), three clusters are evidenced, each composed of points corresponding to the same sample.[18]

In summary, cluster analysis evidences similarity derived from minimizing distances whereas SVD evidences similarity upon inspection of corresponding projections.

These findings demonstrate that time-resolved measurements *alone* contain sufficient information to highlight the differences between surfaces covered with different molecular aggregates.

We now compare the previous results to the standard multi-exponential decay analysis. When the pump pulse excites the system, the relaxation mechanisms manifest themselves invariably in a reflectivity decay that is well mimicked by a sum of exponentially decaying functions. The amplitude and decay time of each function are the fitting parameters. By analyzing the level of residues and the

scaling of fitting parameters, we qualitatively find out that four exponentials are the optimal number to describe the data. Thus, eight parameters, four amplitudes ($a_i, i = 1\ldots4$) and four time decay constants ($\tau_i, i = 1\ldots4$), are needed to fit each experimental trace as $f(t) = a_1 \exp(-t/\tau_1) + a_2 \exp(-t/\tau_2) + a_3 \exp(-t/\tau_3) + a_4 \exp(-t/\tau_4)$. In Fig. 4, the coordinates of each point represent the time decay constants or the amplitudes retrieved from the fitting procedure of a single trace. The color code is the same as the one adopted in Fig. 2.

Regardless of the specific plot one considers in Fig. 4, the formation of clusters identifying different samples is incomplete. Blue triangles (Copoly) never cluster in a visually distinct group, while black circles (Au) and red squares (IgG) cluster to a certain extent in Figs. 4(c) and 4(a) only. Similar considerations can be made for the patterns obtained visualizing data using different formats. The fitting parameters alone are hence not sufficient to group the samples in distinct sets. This points to the power of multidimensional analysis, like the Ward method and the SVD analysis, to capture more similarities than those uncovered by simply comparing fitting parameters.

Our strategy constitutes a change of paradigm with respect to traditional molecular screening methods. We exploit the information encoded in time domain, which are disclosed by multi-dimensional analysis, as opposed to traditional approaches relying on information retrieved from frequency domain techniques. Our results suggest a possible taxonomy of time-resolved spectra aimed at the discrimination of thin molecular layers based on data analysis methods. Our approach entails several advantages. It provides enhanced surface sensitivity and is label-free. The molecular recognition does not rely on the detailed modeling of the mechanism underlying the optical response. The technique has a high data throughput and can be integrated with existing microscopy platforms and lab-on-a chip architectures.

In perspective, a microfluidic lay-out, carved in a polydimethylsiloxane (PDMS) matrix, could be conformally bonded on the prism's Au-coated surface, the latter being functionalized with specific antibodies. The flow of antigens to be sensed will be driven across the chip to several sensing areas—one patch for each antibody—where the pump and probe measurement will be performed. Comparison—via hierarchical cluster analysis and SVD—of the acquired spectra against benchmark time-resolved traces for antigen-bound antibodies will allow identifying the presence of specific antigens and, possibly, their concentration. Within this scheme, the present technique could serve as a high throughput screening method for some pathogens.

Combined with scanning microscopy,[22] the approach outlined in this work would serve as a platform to detect spatial variations in surface chemical properties arising from compositional inhomogeneity of molecular films. Acquisition of a pump and probe trace at each sample's coordinates, followed by association of a false color to each pixel on the basis of clustering analysis, would render a spatial map of the compositional contrast. The typical ASOPS acquisition time per pixel is of the order of few seconds, leading to the acquisition of 32×32 pixel images in less than 1 h.[23]

G.F. acknowledges the support of Università Cattolica del Sacro Cuore through D.2.2 and D.3.1 grants. F.B. and S.P. acknowledge the financial support from the MIUR—Futuro in ricerca 2013 Grant in the frame of the ULTRANANO Project.

[1]A. H. Zewail, J. Phys. Chem. A **104**, 5660 (2000).
[2]W. R. Browne and B. L. Feringa, Annu. Rev. Phys. Chem. **60**, 407 (2009).
[3]P. N. Prasad, *Introduction to Biophotonics* (John Wiley & Sons, 2003).
[4]J. G. Fujimoto and D. Farkas, *Biomedical Optical Imaging* (Oxford University Press, USA, 2009).
[5]A. Diaspro, *Nanoscopy and Multidimensional Optical Fluorescence Microscopy* (CRC Press, 2010).
[6]F. Giavazzi, M. Salina, R. Cerbino, M. Bassi, D. Prosperi, E. Ceccarello, F. Damin, L. Sola, M. Rusnati, M. Chiari, B. Chini, T. Bellini, and M. Buscaglia, Proc. Natl. Acad. Sci. **110**, 9350 (2013).
[7]W. Tan, K. Wang, and T. J. Drake, Curr. Opin. Chem. Biol. **8**, 547 (2004).
[8]M. Sarikaya, C. Tamerler, D. T. Schwartz, and F. Baneyx, Annu. Rev. Mater. Res. **34**, 373 (2004).
[9]G. Pirri, F. Damin, M. Chiari, E. Bontempi, and L. E. Depero, Anal. Chem. **76**, 1352 (2004).
[10]G. Ferrini, L. De Carlo, C. Giannetti, and F. Parmigiani, Opt. Spectrosc. **107**, 464 (2009).
[11]W. Knoll, Annu. Rev. Phys. Chem. **49**, 569 (1998).
[12]*Femtochemistry*, edited by F. C. De Schryver, S. De Feyter, and G. Schweitzer (Wiley-VCH Verlag GmbH, 2002).
[13]R. M. Corn and D. A. Higgins, Chem. Rev. **94**, 107 (1994).
[14]H.-F. Wang, L. Velarde, W. Gan, and L. Fu, Annu. Rev. Phys. Chem. **66**, 189 (2015).
[15]A. C. Pipino, Phys. Rev. Lett. **83**, 3093 (1999).
[16]D. A. Long, A. Cygan, R. Van Zee, M. Okumura, C. Miller, D. Lisak, and J. Hodges, Chem. Phys. Lett. **536**, 1 (2012).
[17]S. G. Kazarian and K. A. Chan, Analyst **138**, 1940 (2013).
[18]See supplementary material at http://dx.doi.org/10.1063/1.4934216 for sample preparation, data analysis procedures, and comments.
[19]J. M. De Sá, *Pattern Recognition: Concepts, Methods, and Applications* (Springer-Verlag, 2001).
[20]I. Jolliffe, *Principal Component Analysis* (Wiley Online Library, 2002).
[21]A. Bartels, R. Cerna, C. Kistner, A. Thoma, F. Hudert, C. Janke, and T. Dekorsy, Rev. Sci. Instrum. **78**, 035107 (2007).
[22]W. Zipfel, R. Williams, and W. Webb, Nat. Biotechnol. **21**, 1369 (2003).
[23]N. Krauß, A. Nast, D. Heinecke, C. Kölbl, H. Barros, and T. Dekorsy, Opt. Express **23**, 2145 (2015).

Discrimination of molecular thin films by Surface-Sensitive Time-Resolved Optical Spectroscopy

Simone Peli,[1,2] Nicola Nembrini,[1,2,3] Francesco Damin,[4] Marcella Chiari,[4] Claudio Giannetti,[1,2] Francesco Banfi,[1,2] and Gabriele Ferrini[1,2,a)]

[1)] *Dipartimento di Matematica e Fisica, Università Cattolica del Sacro Cuore, Brescia I-25121, Italy*

[2)] *Interdisciplinary Laboratories for Advanced Materials Physics (iLamp), Università Cattolica del Sacro Cuore, Brescia I-25121, Italy*

[3)] *Dipartimento di Fisica, Università degli Studi di Milano, Milano I-20122, Italy*

[4)] *Istituto di Chimica del Riconoscimento Molecolare, CNR, Milano, Italy*

I. SAMPLE PREPARATION

A. Coating the surface of prism with copoly(DMA-NAS-MAPS)

Two prisms with thin gold films evaporated on their hypothenuses were treated for ten minutes in an Oxygen Plasma Generator (Harrick Plasma Cleaner) and then immersed for 30 min in a copoly(DMA-NAS-MAPS) solution (1% w/v in 0.8M aqueous solution of ammonium sulfate. The surface of the prisms was then extensively washed with water and dried under vacuum at 80 °C for 15 minutes. Copoly(DMA-NAS-MAPS) was synthesized and characterized as described in previous works[1,2].

B. Immobilization of Streptavidin on the polymer coated surface and incubation with biotinilated IgG

On the surface of a prism, coated with copoly(DMA-NAS-MAPS), a 0.2 mg/mL solution of streptavidin (Sigma) in PBS (Phosphate buffered saline, 10mM phosphate buffer, 2.7mM KCl, 137mM NaCl; pH 7.4) was spotted by means of an automated noncontact dispensing system (sciFLEXARRAYER S5; Scienion AG). The entire surface was coated by merging 200-μm spots of protein solution. After the spotting, the prisms were stored overnight in a humid chamber at RT. The unreacted N-hydroxysuccinimide of NAS was blocked with a solution of 5% ethanolamine in Tris-HCl buffer solution for 1h and washed with H_2O. The prism was incubated with a 300ng/mL solution of biotin-conjugated goat anti-rabbit IgG (Li StarFish, PA, USA) in incubation buffer (50mM Tris/Hcl pH 7.6; 150mM NaCl; 0.02% Tween 20) for 1 hour at room temperature and then washed with PBS for 10 minutes.

[a)] Electronic mail: gabriele.ferrini@unicatt.it

II. DATA ANALYSIS PROCEDURES

A. Fitting procedures

The traces have been pre-processed. Each raw time-trace contains 40000 points sampled with a 100 fs period. The traces have been evenly decimated to reduce the length of the time-resolved spectra, without information loss, to a computationally manageable length of 2000 points. We verified that varying the number of points in a wide range (500 - 15000) the results of successive analysis were not affected. The average value of the trace before the pump is the reference level, that is assigned to zero (no reflectivity variation due to the pump). The maximum value of each trace is normalized to one and used as a reference for the zero delay. The fitting procedure uses as a fitting function the sum of four exponentials as $f(t) = a_1\exp(t/\tau_1) + a_2\exp(t/\tau_2) + a_3\exp(t/\tau_3) + a_4\exp(t/\tau_4)$. The fit converges for all the traces. The fit and the residues (the difference between the traces and the fitting functions) for three representative traces are shown in Fig. S1. The traces used are the same shown in Fig. 2 in the article, chosen to represent an optimal noise to signal ratio (trace 10 for IgG), an intermediate noise to signal ratio (trace 1 for Au) and a trace with evident electronic noise (trace 6 for Copoly), that is clearly visible in the residues. Refer to the article for comments. The values of the parameters obtained for all traces in the fitting procedure are synthesised in Fig. 4 of the article. The presence of two negative decay constant in Fig. 4 associated with long decay times (τ_4), those in the 5-10 ns range, are due to a small systematic background trends over a time span actually longer than the maximum investigated delay, 3.8 ns. These negative decay constants are associated to small amplitudes, and their presence is of no significance for physical interpretation.

B. Hierarchical cluster analysis

The total 13 experimental traces have been organized in a 2000×13 data matrix X. Columns of X correspond to experimental traces, and rows to measurements at different delays. To measure the similarity among spectra, we aggregate the data using a hierar-

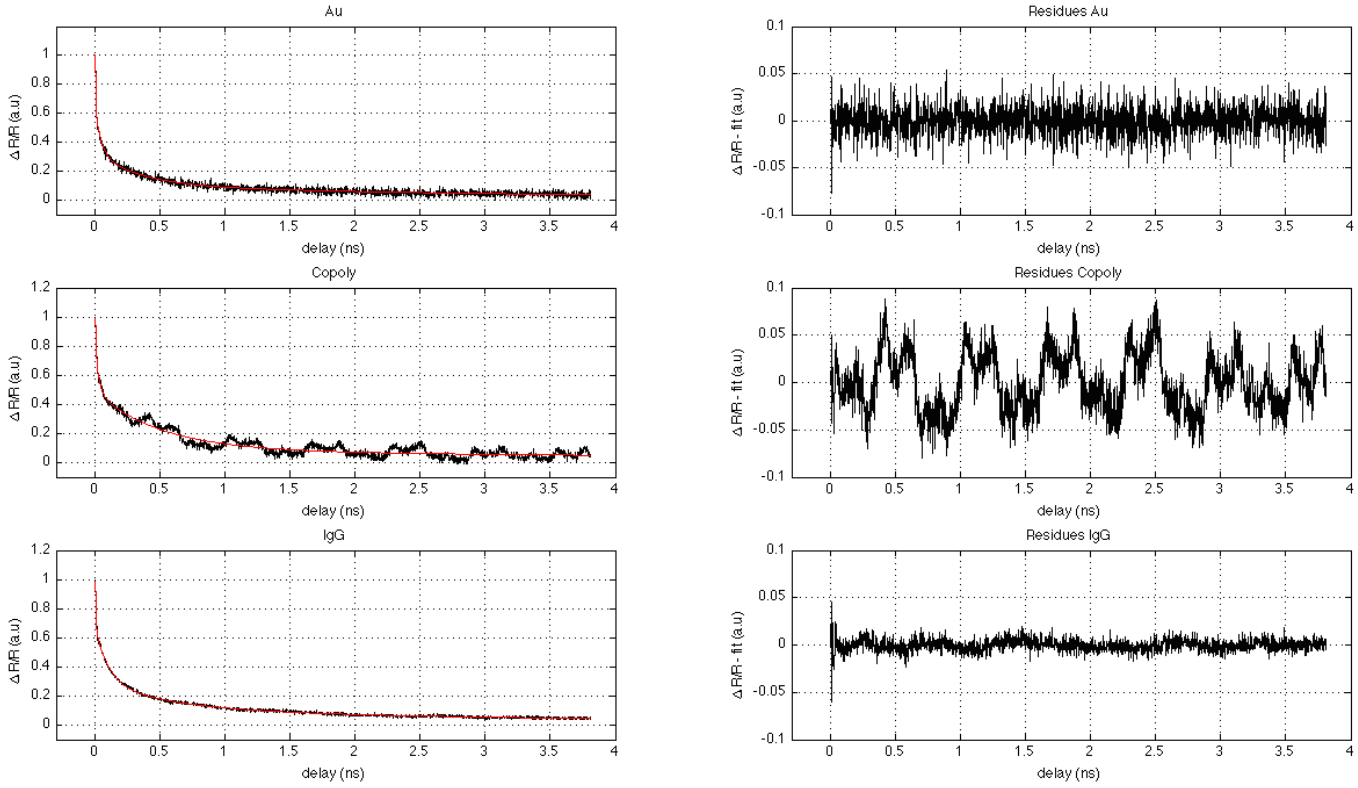

FIG. S1. Fitting results for Au , Copoly, IgG on the left column and corresponding residues on the right column

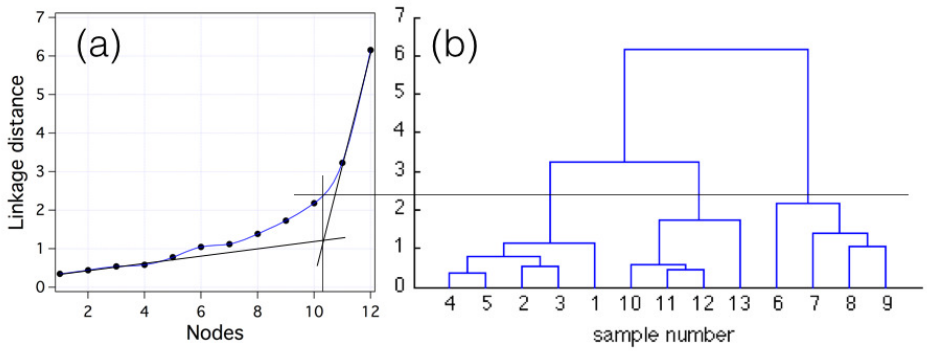

FIG. S2. (a) Clustering schedule graph. (b) vertical icicle plot for the time-resolved data. The intercept in (a) show that the linkage distance corresponding to the best cluster solution cut the vertical icicle where three clusters are present. The clusters groups together the three different samples, Au (1:5), Copoly (6:9) and IgG (10:13).

chical cluster analysis known as Ward's minimum variance method[3]. First the Euclidean distance between all pairs of objects (the 13 experimental traces) in the m-by-n data matrix X ($m = 2000$, $n = 13$ in our case) is calculated. The results are organized in a vector D of length $n(n-1)/2$, corresponding to pairs of experimental traces in X. The distances are arranged in the order $(2,1),(3,1),...,(n,1),(3,2),...,(n,2),...,(n,n-1)$. From the distances in D an agglomerative hierarchical cluster tree is formed using the Ward method. In Ward's method, the sum of the squared within-cluster distances, for the resulting merged cluster, is computed. The within-cluster squared distance is defined as the sum of the squares of the distances between all objects in the cluster and the centroid of the cluster. At each step the two clusters that merge are the ones that contribute to the smallest increase of the overall sum of the squared within-cluster distances. The hierarchical sequence so obtained has the form of a binary tree with two branches for each tree node. The binary tree can be represented

as a dendrogram (as Fig. 3a in the article) or as a vertical icicle plot shown in Fig. S2b. Fig. S2a shows the clustering schedule graph, that plots the number of tree nodes vs linkage distance. A cubic spline interpolates the data. The clustering schedule graph can be used to select the best cluster solution using reasonable assumptions, as follows. Two trend lines represent the plateau and the jump that usually characterize the clustering schedule graph as an abrupt raise in the linkage distance. The intercept point identify a node number, in our case between 10 and 11, corresponding to a linkage distance on the spline curve that cut the icicle plot at a level where three clusters constitute the best solution.

C. Singular value decomposition

The 2000×13 data matrix X is composed of $n = 13$ column vectors $\mathbf{x}_i$ of length $m = 2000$ representing the experimental traces. The Singular Value Decomposition (SVD) equation for the data matrix is $X = USV^T$. The columns of matrix U are the orthonormal eigenvectors $\mathbf{u}_k$ that span the space where the column vectors in X are represented. The diagonal matrix S contains the associated eigenvalues. The elements (k, i) of matrix $M = SV^T$ are the projections $\mathbf{u}_k \cdot \mathbf{x}_i$ of the i-th trace on the k-th eigenvector. The reconstruction of $\mathbf{x}_i$ is given by $\mathbf{x}_i = \sum_{k=1}^{n} v_{ik} s_k \mathbf{u}_k$. It is possible to approximate the data matrix by reducing the number of eigenvectors used to reconstruct the traces. In our case we use only the two eigenvectors with the highest eigenvalues to approximately reconstruct the traces.

D. Physical Insigths

As explained in the text, the detailed and quantitative analysis of the physical mechanism responsible for the optical response in pump-probe experiments need not be known to interpret data with the applied statistical methods. However, the general physical principles are known and we here briefly comment on them.

The evanescent probe senses a variation of the refractive index induced by the pump beam inside the thin molecular film and the vibrationally excited, perturbed surface layer of the substrate, known as the selvedge. In the evanescent wave configuration the internal reflection experienced by the probe is equivalent to a transmission through an effective thickness of an absorbing medium, causing the probe absorption[4]. Both the real and imaginary parts of the refractive index are responsible for the variation of the probe absorption. The refractive index may depend for instance on temperature[5] and charge excitation inside the molecules. The variations due to charge excitation are fast (on the 1-10 ps time scale) while the excitations due to heat transfer are slower (on the 100 ps - ns time scale)[5]. The pump modifies both the temperature and the charge distribution in the molecules and the substrate. Since different molecular layer possess different thermodynamical properties (thermal conductivities, specific heat and dielectric constant dependence on temperature) it is reasonable to expect that the temporal response of the probe to the pump excitation is rather unique to the specific chemical compound and its organization. Since the same molecules organized in different structures may have different electronic and thermal properties, the resulting compounds will be optically different and discriminated by the time-resolved evanescent absorption spectroscopy. We are exploiting the complex interplay that leads to the variation of absorption in time subsequent to a pump excitation.

Finally, it is important to note that, based on the pump fluence and an estimate of the thin gold film absorption, the temperature increase in our case is less than 10 K. Thus we expect that the gold film heating is not able to damage or modify the bound biomolecules.

ACKNOWLEDGMENTS

G. F. acknowledges the support of Università Cattolica del Sacro Cuore through D.2.2 grants. F.B. and S.P acknowledge financial support from the MIUR - "Futuro in ricerca 2013" Grant in the frame of the ULTRANANO Project.

[1] L. Sola and M. Chiari, Journal of Chromatography A **1270**, 324 (2012).
[2] A. Yalçın, F. Damin, E. Özkumur, G. di Carlo, B. B. Goldberg, M. Chiari, and M. S. Ünlü, Analytical chemistry **81**, 625 (2008).
[3] J. M. De Sá, *Pattern recognition: concepts, methods, and applications* (Springer-Verlag, 2001).
[4] N. Harrick and F. Du Pré, Applied optics **5**, 1739 (1966).
[5] T. Stoll, P. Maioli, A. Crut, S. Rodal-Cedeira, I. Pastoriza-Santos, F. Vallée, and N. Del Fatti, The Journal of Physical Chemistry C **119**, 12757 (2015).